Shape-Persistent Macrocycles with Intraannular Polar Groups: Synthesis, Liquid Crystallinity, and 2D Organization

Matthias Fischer,† Günter Lieser,*,† Almut Rapp,† Ingo Schnell,*,† Wael Mamdouh,‡
Steven De Feyter,*,‡ Frans C. De Schryver,‡ and Sigurd Höger*,†,§

*Contribution from the Max Planck Institute for Polymer Research, Ackermannweg 10,
D-55128 Mainz, Germany, and Katholieke Universiteit Leuven (K.U.Leuven),
Department of Chemistry, Celestijnenlaan 200 F, B-3001 Leuven, Belgium*

Received September 12, 2003; E-mail: hoeger@chemie.uni-karlsruhe.de

Abstract: The synthesis of macrocycles with intraannular polar ester groups and extraannular oligo-alkyl groups is described. The compounds exhibit stable liquid crystalline phases showing fan-shaped textures under the polarizing microscope, typical for a columnar order of the molecules. X-ray powder diffraction data of the LC phase indicate that the unit cell contains two symmetry-related units, a feature pointing most probably to a restricted rotation of the macrocycles within a stack. The X-ray data were further supported by solid-state NMR experiments, showing that the rigid core of the compounds does not rotate with kHz or higher frequencies within the column in the LC phase. Apart from the organization of the molecules in the LC phase, the 2D organization of the macrocycles at the solvent—highly oriented pyrolytic graphite (HOPG) interface was investigated and showed that these compounds are capable of nanofunctionalizing the HOPG surface in the multinanometer regime.

Introduction

The investigation of shape-persistent macrocycles has become a topic of growing interest during the past decade. Apart from the synthesis, special emphasis is given to the supramolecular aspects of these compounds. These include, among others, the binding of appropriate guest molecules, the pattern formation at interfaces, and the organization of the molecules in the crystalline and in the liquid crystalline state.[1] Liquid crystalline materials based on disklike mesogens (discotic liquid crystals) were first described by Chandrasekhar more than 25 years ago.[2] They are, in general, composed of a disklike or macrocyclic core and flexible side groups pointing to the outside.[3] Apart from their possible applications in display technology,[4] they have attracted much attention since Adam et al. found that discotic liquid crystals based on a polycyclic aromatic core exhibit high mobilities for photoinduced charge carriers in the columnar

phase.[5] Subsequent investigations in this area led recently to the fabrication of highly efficient photovoltaic elements.[6]

If the mesogenic unit of the liquid crystal is a macrocycle, the arrangement of the mesogens in an axial stack might form a hollow column leading to a tubular superstructure.[7] A necessary prerequisite for the formation of a supramolecular hollow columnar structure is to prevent the macrocycles from collapsing. In flexible ring systems, this can be accomplished by the formation of host—guest complexes.[8] However, the formation of tubular superstructures from shape-persistent macrocycles seems to be more attractive because these mesogens are, per se, noncollapsed.[9] Therefore, functional groups inside the rings (intraannular substituents) are not blocked by the interaction with guest molecules but remain rather free, leading to the formation of intraannular functionalized nanotubes.[10,11] As an additional feature unavailable in discotic liquid crystals based on disklike molecules, shape-persistent macrocycles allow

---

† Max Planck Institute for Polymer Research.

‡ Katholieke Universiteit Leuven (K. U. Leuven).

§ New address: Polymer Institute, Universität Karlsruhe, Engesserstr. 18, D-76131 Karlsruhe, Germany.

(1) For recent reviews on shape-persistent macrocycles, see for example: (a) Moore, J. S. *Acc. Chem. Res.* **1997**, *30*, 402—413. (b) Höger, S. *J. Polym. Sci., Part A: Polym. Chem.* **1999**, *37*, 2685—2698. (c) Haley, M. M.; Pak, J. J.; Brand, S. C. *Top. Curr. Chem.* **1999**, *201*, 81—130. (d) Grave, C.; Schlüter, A. D. *Eur. J. Org. Chem.* **2002**, 3075—3098. (e) Zhao, D.; Moore, J. S. *Chem. Commun.* **2003**, 807—818.

(2) (a) Chandrasekhar, S.; Sadashiva, B. K.; Suresh, K. A. *Pramana* **1977**, *7*, 471—480. (b) Chandrasekhar, S. In *Handbook of Liquid Crystals*; Demus, D., Goodby, J., Gray, G. W., Spiess, H.-W., Vill, V., Eds.; Wiley-VCH: Weinheim, Germany, 1998; Vol. 2B, pp 749—780. (c) Bushby, R. J.; Lozman, O. R. *Curr. Opin. Colloid Interface Sci.* **2002**, *7*, 343—354.

(3) For an exception of this rule, see: Höger, S.; Enkelmann, V.; Bonrad, K.; Tschierske, C. *Angew. Chem.* **2000**, *112*, 2356—2358; *Angew. Chem., Int. Ed.* **2000**, *39*, 2268—2270.

(4) Kumar, S.; Varshney, S. K. *Angew. Chem.* **2000**, *112*, 3270—3272; *Angew. Chem., Int. Ed.* **2000**, *39*, 3140—3142.

(5) Adam, D.; Schuhmacher, P.; Simmerer, J.; Häussling, L.; Siemensmeyer, K.; Etzbach, K. H.; Ringsdorf, H.; Haarer, D. *Nature* **1994**, *371*, 141—143.

(6) (a) Ito, S.; Wehmeier, M.; Brand, J. D.; Kübel, C.; Epsch, R.; Rabe, J. P.; Müllen, K. *Chem.—Eur. J.* **2000**, *6*, 4327—4342. (b) Schmidt-Mende, L.; Fechtenkötter, A.; Müllen, K.; Moons, E.; Friend, R. H.; MacKenzie, J. D. *Science* **2001**, *293*, 1119—1122.

(7) Behr, J.-P.; Lehn, J.-M.; Dock, A.-C.; Moras, D. *Nature* **1982**, *295*, 526—527.

(8) (a) Lehn, J. M.; Malthête, J.; Levelut, A. M. *J. Chem. Soc., Chem. Commun.* **1985**, 1794—1796. (b) Lattermann, G. *Mol. Cryst. Liq. Cryst.* **1990**, *182B*, 299—311. (c) Liebmann, A.; Mertesdorf, C.; Plesnivy, T.; Ringsdorf, H.; Wendorff, J. H.; *Angew. Chem.* **1991**, *103*, 1358—1361; *Angew. Chem., Int. Ed. Engl.* **1991**, *30*, 1375—1377.

(9) (a) Mindyuk, O. Y.; Stetzer, M. R.; Heiney, P. A.; Nelson, J. C.; Moore, J. S. *Adv. Mater.* **1998**, *10*, 1363—1366. (b) Zhang, J.; Moore, J. S. *J. Am. Chem. Soc.* **1994**, *116*, 2655—2656.

(10) For the concept of intraannular functional groups, see for example: (a) Vögtle, F.; Neumann, P. *Tetrahedron* **1970**, *26*, 5299—5318. (b) Weber, E.; Vögtle, F. *Chem. Ber.* **1976**, *109*, 1803—1831.
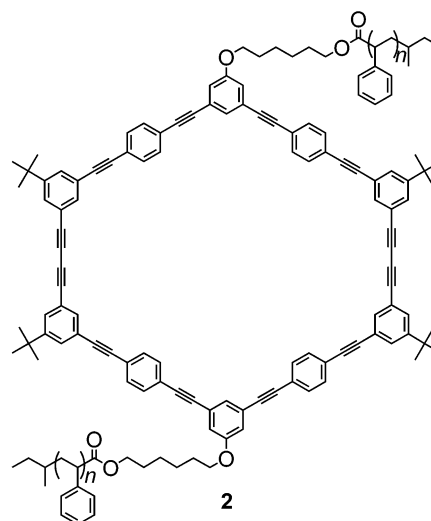
Chart 1

1a: R =

1b: R =

1c: R =

Chart 2

2
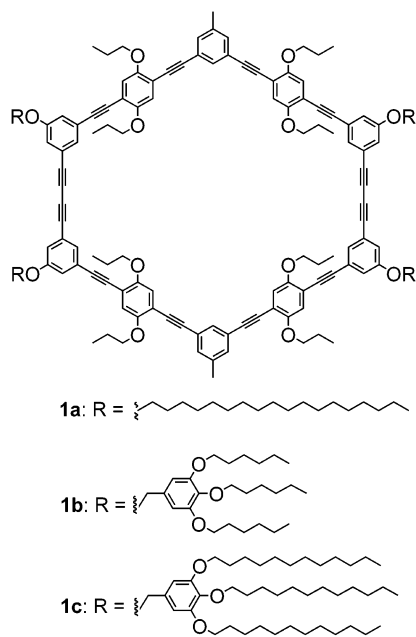
the investigation of the influence of intraannular substituents (e.g., size, polarity, etc.) on the thermal behavior of the materials, while other molecular parameters (e.g., core dimension, grafting positions, length of the aliphatic tails, etc.) can be kept constant.[12]

Recently, we described shape-persistent macrocycles **1a**−**c** with alkyl and oligo-alkyl substituents of defined size (Chart 1).[13] At first glance, these compounds match the design principle of discotic liquid crystals, namely, a stiff core unit surrounded by a flexible periphery. However, none of the compounds exhibits a stable thermotropic LC phase. In addition, the formation of a tubular superstructure by the aggregation of the macrocycles in solution could also not be observed. An aggregation of the macrocycles in CH_2Cl_2 could be induced by the addition of hexane, which is a nonsolvent for the rigid macrocyclic core, but restricted compound solubility prevents the observation of high aggregation constants.[14] The solubility

problem could be solved by attaching polystyrene substituents to the macrocyclic backbone, as in the macrocycles **2** (Chart 2).[15]

These compounds dissolve even in cyclohexane and form supramolecular tubes in solution, depending on the size of the attached polystyrene, as has been investigated by scattering as well as imaging methods. However, none of these coil−ring−coil block copolymers exhibit a thermotropic columnar mesophase. These observations lead us to the assumption that the large internal void inside the noncollapsible macrocycles prevents the system from forming a stable thermotropic mesophase due to the frustration between the molecular anisotropy and the empty space inside the rings: It can be assumed that the empty space inside the rings is not filled by backfolding of the extraannular substituents attached to the periphery of **1** or **2**. Hence, the alkyl (oligo-styryl) groups of adjacent rings have to point inside the macrocycles, and the competition between orientational correlation of the rigid parts of the molecule and the necessity of the side groups to fill the interior of adjacent rings prevent the formation of a stable LC phase. This hypothesis is further supported by the observation that isomers of **1a** with a filled cavity do exhibit a stable mesophase.[3] However, an alternative explanation for the absence of a stable thermotropic mesophase in **1** and **2** could be the incorrect balance between the core dimension and the size of the flexible periphery.[16]

To get a deeper insight into the molecular requirements for the formation of a stable LC phase in these macrocycles, we intended to investigate derivatives of **1** in which the interior of the mesogenic unit is filled by intraannular polar groups. If the balance between rigid and flexible parts of the molecule is correct, the filling of the interior should allow the formation of a stable LC phase. Additionally, the intermolecular interaction of the polar intraannular groups should prevent the molecules from sliding relative to each other and, in this way, stabilize a columnar packing motive in the mesophase.

(11) For shape-persistent macrocycles containing intraannular functional groups, see for example: (a) Anderson, H. L.; Sanders, J. K. M. *J. Chem. Soc., Chem. Commun.* **1992**, 946−947. (b) Anderson, S.; Neidlein, U.; Gramlich, V.; Diederich, F. *Angew. Chem.* **1995**, *107*, 1722−1726; *Angew. Chem., Int. Ed. Engl.* **1995**, *34*, 1596−1600. (c) Morrison, D. L.; Höger, S. *J. Chem. Soc., Chem. Commun.* **1996**, 2313−2314. (d) Tobe, Y.; Utsumi, N.; Kawabata, K.; Nagano, A.; Naemura, K. *Angew. Chem.* **1998**, *110*, 1347−1349; *Angew. Chem., Int. Ed.* **1998**, *37*, 1285−1287. (e) Höger, S.; Meckenstock, A.-D. *Chem.−Eur. J.* **1999**, *5*, 1686−1691. (f) Lehman, U.; Schlüter, A. D. *Eur. J. Org. Chem.* **2000**, 3483−3487. (g) Hosokawa, Y.; Kawase, T.; Oda, M. *J. Chem. Soc., Chem. Commun.* **2001**, 1948−1949. (h) Höger, S.; Morrison, D. L.; Enkelmann, V. *J. Am. Chem. Soc.* **2002**, *124*, 6734−6736. (i) Fischer, M.; Höger, S. *Eur. J. Org. Chem.* **2003**, 441−446. (j) Grave, C.; Lentz, D.; Schäfer, A.; Samori, P.; Rabe, J. P.; Franke, P.; Schlüter, A. D. *J. Am. Chem. Soc.* **2003**, *125*, 6907−6918. (k) Fischer, M.; Höger, S. *Tetrahedron* **2003**, *59*, 9441−9446.

(12) Heinrich, B.; Praefke, K.; Guillon, D. *J. Mater. Chem.* **1997**, *7*, 1363−1372.

(13) Höger, S.; Bonrad, K.; Mourran, A.; Beginn, U.; Möller, M. *J. Am. Chem. Soc.* **2001**, *123*, 5651−5659.

(14) For the aggregation of large macrocycles, see, for example: (a) Zhang, J.; Moore, J. S. *J. Am. Chem. Soc.* **1992**, *114*, 9701−9702. (b) Shetty, A. S.; Zhang, J.; Moore, J. S. *J. Am. Chem. Soc.* **1996**, *118*, 1019. (c) Tobe, Y.; Nagano, A.; Kawabata, K.; Sonoda, M.; Naemura, K. *Org. Lett.* **2000**, *2*, 3265−3268. (d) Nakamura, K.; Okubo, H.; Yamaguchi, M. *Org. Lett.* **2000**, *2*, 3265. (e) Tobe, Y.; Utsumi, N.; Kawabata, K.; Nagano, A.; Adachi, K.; Araki, S.; Sonoda, M.; Hirose, K.; Nakamura, K. *J. Am. Chem. Soc.* **2002**, *124*, 5350−5364. (f) Zhao, D.; Moore, J. S. *J. Org. Chem.* **2002**, *67*, 3548−3554. (g) Saiki, Y.; Sugiura, H.; Nakamura, K.; Yamaguchi, M.; Hoshi, T.; Anzai, J. *J. Am. Chem. Soc.* **2003**, *125*, 9268−9269.

(15) (a) Rosselli, S.; Ramminger, A.-D.; Wagner, T.; Silier, B.; Wiegand, S.; Häuβler, W.; Lieser, G.; Scheumann, V.; Höger, S. *Angew. Chem.* **2001**, *113*, 3234−3237; *Angew. Chem., Int. Ed.* **2001**, *40*, 3138−3141. (b) Höger, S.; Bonrad, K.; Rosselli, S.; Meckenstock, A.-D.; Wagner, T.; Silier, B.; Wiegand, S.; Häuβler, W.; Lieser, G.; Scheumann, V. *Macromol. Symp.* **2002**, *177*, 185−191. (c) Rosselli, S.; Ramminger, A.-D.; Wagner, T.; Lieser, G.; Höger, S. *Chem.−Eur. J.* **2003**, *9*, 3481−3491.

(16) Kohne, B.; Praefcke, K. *Chem.−Ztg.* **1985**, *109*, 121−127.

Scheme 1 [a]

3a: R =

3b: R =
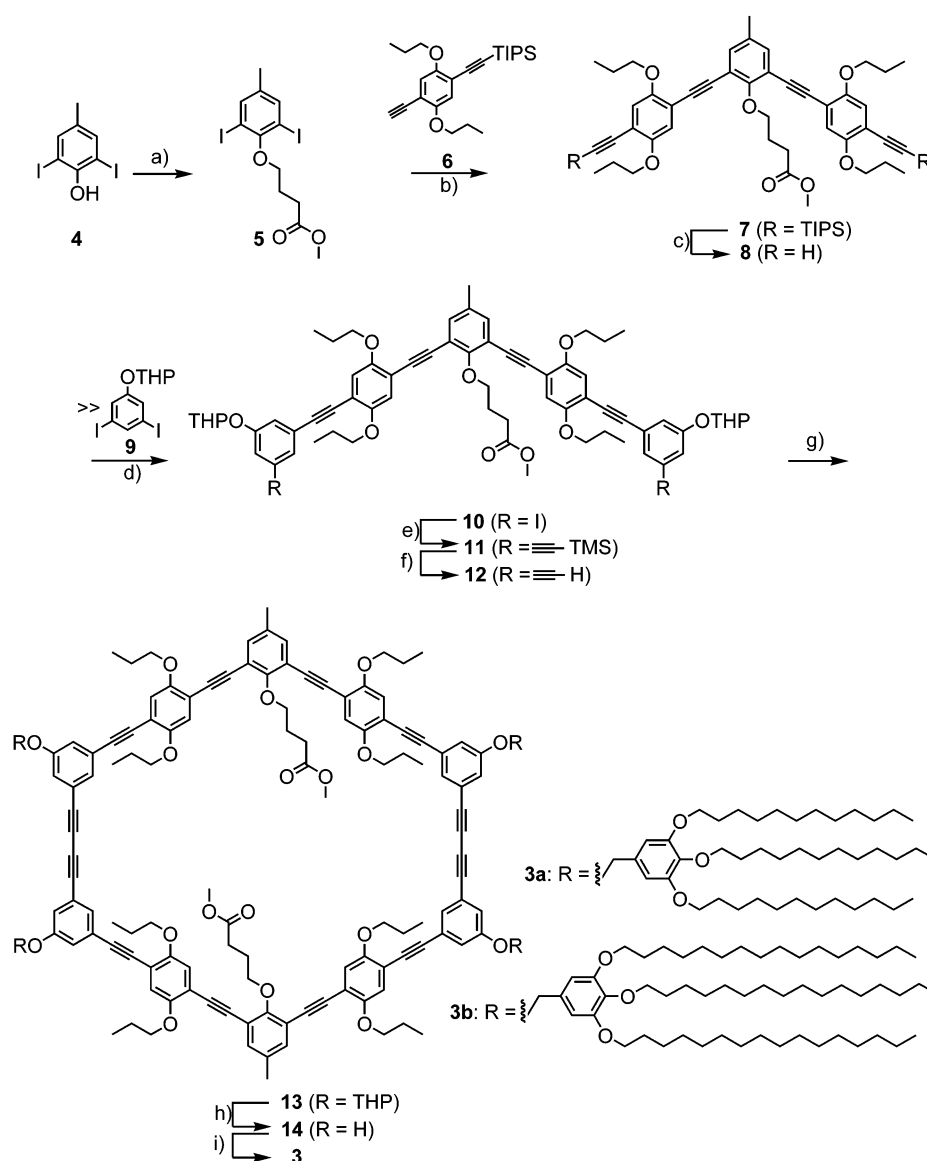
[a] (a) 4-Bromotrimethylorthobutyrate, K$_2$CO$_3$, DMF (73%). (b) PdCl$_2$(PPh$_3$)$_2$, CuI, NEt$_3$ (87%). (c) Bu$_4$NF, THF/H$_2$O (74%). (d) PdCl$_2$(PPh$_3$)$_2$, CuI, NEt$_3$/THF (81%). (e) TMS-acetylene, PdCl$_2$(PPh$_3$)$_2$, CuI, piperidine (86%). (f) K$_2$CO$_3$, MeOH/THF (89%). (g) CuCl, CuCl$_2$, pyridine, 29%. (h) *p*-TsOH, MeOH, CHCl$_3$, 68%. (i) tris(alkoxy)benzyl chloride, K$_2$CO$_3$, DMF, 30−48%.

Apart from the formation of 1D superstructures, shape-persistent macrocycles can be the basis for regular 2D structures. In the case of extraannular functionalized macrocycles, it has been shown that the interaction of the polar groups in the solid state can lead to the formation of (quasi) 2D structures.[17] However, in that case, the functional groups are essential for the superstructure stabilization and do not remain free for the recognition of additional objects. Pattern formation at interfaces is an attractive alternative because it does not rely on the specific functional group interaction. Therefore, those remain free and might be used for the creation of supramolecular 3D structures, using the 2D structure as a template. Previous experiments have shown that **1c** forms regular 2D structures at the surface of highly oriented pyrolytic graphite (HOPG). In that case, the driving force for the pattern formation is purely dissipative.[13] Therefore, similar pattern formation of intraannular function-

alized macrocycles should offer additional features since it leads not only to a *nanopatterned* surface but also to a *functionalized nanopatterned* surface using the intraannular anchor groups for the epitaxially induced 3D superstructure formation.[18]

Results and Discussion

Synthesis and Characterization. Target structures of our investigations are the macrocycles **3a** and **3b**, which can be viewed as intraannular functionalized analogues of the previously described compound **1**. The synthesis of the macrocycles is outlined in Scheme 1.

2,6-Diiodo-4-methylphenol (**4**) was alkylated by treatment with 4-bromo-trimethylorthobutyrate to yield the ester **5** in 73%

(17) Venkataramen, D.; Lee, S.; Zhang, J.; Moore, J. S. *Nature* **1994**, *371*, 591−593.

(18) For a recent report of the functionalization of an Au(111) surface see: Pan, G.-B.; Liu, J.-M.; Zhang, H.-M.; Wan, L.-J.; Zheng, Q.-Y.; Bai, C.-L. *Angew. Chem.* **2003**, *115*, 2853−2857; *Angew. Chem., Int. Ed.* **2003**, *42*, 2747−2751.
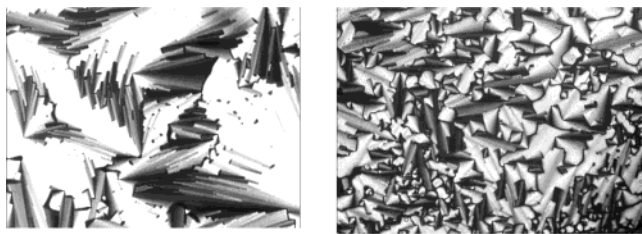
Figure 1. Texture of **3a** (left, 150 °C) and **3b** (right, 110 °C) between crossed polarizers.

yield.[19] Palladium-catalyzed Hagihara–Sonogashira coupling with the monoprotected bisacetylene **6** and subsequent desilylation by treating **7** (87%) with Bu₄NF gave the bisacetylene **8** (74%). As described previously, the basicity of the fluoride was reduced by adding about 5% of water to the THF.[11e] Reaction of **8** with a 7-fold excess of the THP-protected diiodophenol **9** gave the diiodo compound **10** in 81% yield. The excess of **9** was nearly quantitatively recovered and could be used for subsequent coupling reactions. Coupling of **10** with trimethylsilyl (TMS)-acetylene yielded **11** (86%), which was desilylated with K₂CO₃ to give **12** (89%). The statistical intermolecular oxidative dimerization of **12** was performed by slow addition of a solution of **12** in pyridine to a suspension of CuCl and CuCl₂ in the same solvent at 60 °C, a compromise between increased coupling rate and decreased product stability at elevated temperatures.[20] The crude cyclization product (dimer content ca. 60% (GPC)) was purified by radial chromatography to give pure **13** in 29% isolated yield. Acid-catalyzed deprotection of the THP groups gave the tetraphenol **14** (68%). Alkylation of **14** with the benzyl chlorides **15a** and **15b** gave the oligo-alkyl-substituted macrocycles **3a** and **3b**, respectively.[21] **3a** and **3b** were characterized by elemental analysis, NMR spectroscopy, gel permeation chromatography (GPC), and matrix-assisted laser desorption ionization time-of-flight (MALDI TOF) spectroscopy. In solution, the ¹H NMR spectra of the compounds show molecules with a high degree of symmetry, as expected from the molecular structure (Supporting Information). Additionally, the results of the GPC analysis indicate that the compounds do not contain incompletely alkylated impurities. The assigned structure based on the NMR and GPC data was verified by the results of the mass spectroscopic analysis. The MALDI TOF spectra of **3a** and **3b** show the masses of single peaks corresponding to the masses of the macrocyclic Ag⁺ adducts (Supporting Information).

Thermal Behavior. Of special interest was the investigation of the thermotropic behavior of the oligo-alkyl-substituted macrocycles **3a** and **3b**, which was performed by optical polarization microscopy (OPM) and differential scanning calorimetry (DSC). Both compounds exhibit stable mesophases and show, in the LC phase, beautiful fan-shaped textures under the polarizing microscope, which are typical for a columnar order of the molecules (Figure 1). **3a** melts at 93 °C ($\Delta H_t = 176$ kJ mol⁻¹; second heating) to form a LC phase that becomes isotropic at 195 °C. As expected, the melting point of **3b** is lower (82 °C; $\Delta H_t = 151$ kJ mol⁻¹; second heating), and also,
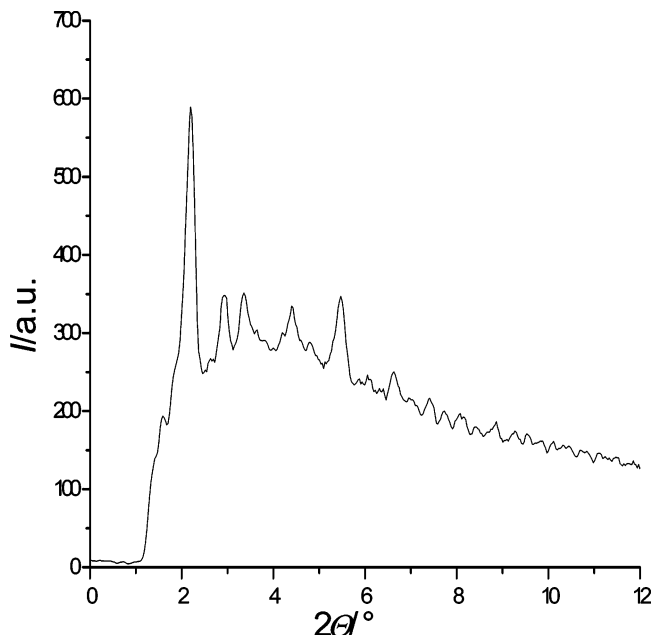
Figure 2. X-ray powder diffractogram of **3a** at 120 °C.

the temperature range of the LC phase that is formed is smaller, showing a clearing temperature of 145 °C.[22]

The observation of a stable LC phase in **3a**, that cannot be observed in **1c**, shows that the balance between the core dimension and the flexible periphery in these molecules were correct, but the large internal void in **1c** destabilizes a thermotropic mesophase. It is also interesting to note that the melting point of **3a** is about 30 °C below the melting point of **1c**, although the former contains additional (intraannular) polar ester groups. This is another indication for our previously reported hypothesis that the large empty interior in these shape-persistent macrocycles can act as a physical cross-link.[3]

X-ray and Electron Diffraction. To obtain a better insight into the supramolecular organization of the macrocycles in the liquid crystalline and, for comparison, in the solid state, a combined X-ray and electron diffraction study was performed. In X-ray powder diffraction diagrams of **3a** and **3b** (measured in transmission), several reflections are seen in the LC phase in the range up to a scattering angle of 12° (Figure 2; Table 1).

Because stacking of the macrocycles can be suggested with a distance between the rings of only a few Å, the *d* values of the reflections in the measured range are too high to be indexed with $l \neq 0$.[15c] All the data match an oblique net with the basal periodicities $a = 67.6$ and $b = 42.5$ Å and an angle between the main directions $\gamma = 109.6°$ for **3a** and $a = 72.6$, $b = 45.6$ Å, and $\gamma = 98.5°$ for **3b**. In both compounds, two stacks of the macrocycles run through one mesh of this oblique net ($Z = 2$). Keeping in mind that this basal net belongs to a liquid crystal, the fact that a possible unit cell contains two symmetry-related units is rather surprising and requires that both stacks be discriminated from each other also in the liquid crystalline state (Figure 3).[9a,23,24] This feature points most probably to a restricted rotation of the macrocycles within the stacks.

(19) Attempts to obtain **5** by the alkylation of **4** with ethyl 4-bromobutyrate failed and gave only unidentified dark products.
(20) Höger, S.; Bonrad, K.; Karcher, L.; Meckenstock, A.-D. *J. Org. Chem.* **2000**, *65*, 1588–1589.
(21) Balagurusamy, V. S. K.; Ungar, G.; Percec, V.; Johansson, G. *J. Am. Chem. Soc.* **1997**, *119*, 1539–1555.
(22) Although different heating and cooling rates were employed, we were not able to observe the LC-isotropic transition in the DSC.
(23) Frank, F. C.; Chandrasekhar, S. *J. Phys. (Paris)* **1980**, *41*, 1285–1288.
(24) Levelut, A. M. *J. Chim. Phys.* **1983**, *80*, 149–161.

Table 1. Reflections of **3a** (at 120 °C) and **3b** (at 110 °C) in the Liquid Crystalline State

$2\vartheta_{obsd}$ [deg]	$2\vartheta_{calcd}$ [deg]	indexing *hk*	d_{calcd} [Å]	$2\vartheta_{obsd}$ [deg]	$2\vartheta_{calcd}$ [deg]	indexing *hk*	d_{calcd} [Å]
	3a[a]				**3b**[b]		
1.39	1.386	10	63.7	1.18	1.229	10	71.8
2.19	2.175	$\bar{1}1$	40.6	1.92	1.958	01	45.1
	2.204	01	40.1	2.16	2.153	$\bar{1}1$	41.0
2.92	2.772	20	31.8	2.52	2.459	20	35.9
	2.906	$\bar{2}1$	30.4		2.462	11	35.9
4.20	4.154	$\bar{1}2$	21.3	2.92	2.908	$\bar{2}1$	30.4
	4.158	30	21.2	3.94	3.917	02	22.6
4.40	4.350	$\bar{2}2$	20.3	4.81	4.919	40	17.9
	4.408	02	20.0		4.925	22	17.9
4.80	4.944	$\bar{3}2$	17.9	5.89	5.878	03	15.0
5.47	5.545	40	15.9	6.80	6.700	23	13.2

[a] Lattice base $a = 67.6$ Å, $b = 42.5$ Å, $\gamma = 109.6°$, $Z = 2$ (some reflections superimpose without visible separation). [b] Lattice base $a = 72.6$ Å, $b = 45.6$ Å, $\gamma = 98.5°$, $Z = 2$ (some reflections superimpose without visible separation).
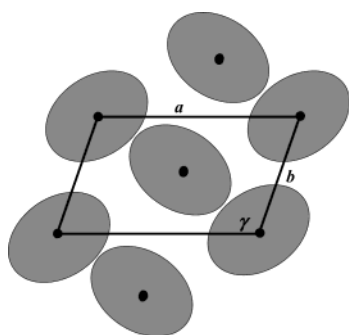
Figure 3. Two-dimensional lattice symmetry in **3a** and **3b**, projection along the stack axes.

In the X-ray diffraction diagram of a powder, even in an extended angular range, no trace of any feature has been found that could be attributed to a periodicity along the suggested stacks. The hope to orient the sample to see something similar to a fiber diagram when the sample was cooled slowly in the mark capillary was in vain. Also, for the solids we disposed of powder data only. They are compiled in Table 2.

Under the assumption of a monoclinic lattice (see below), the X-ray reflections of the solids can be explained by a lattice with the parameters $a = 55.7$ Å, $b = 47.6$ Å, $c = 4.8$ Å, $\gamma = 99.8°$ ($Z = 2$), and $\rho = 1.17$ g cm^{-3} for **3a** and $a = 62.7$ Å, $b = 48.7$ Å, $c = 4.8$ Å, $\gamma = 97.8°$ ($Z = 2$), and $\rho = 1.16$ g cm^{-3} for **3b** (also for the solid state, the parameter c could not be determined by X-ray data. Electron diffraction patterns (see below) display continuous layer lines that would not show up in X-ray powder diagrams as distinct reflections). During the phase transition from the liquid crystalline to the crystalline state, the a-parameter is shortened and the b-parameter is extended. The angle γ has only changed significantly for **3a**.

Additional information on the solid-state structure of **3a** and **3b** was obtained by electron diffraction. In contrast to the X-ray experiments, in the electron diffraction studies the specimen scale allowed for observation of a fiberlike diagram in restricted areas. Recording of an electron diffractogram at ambient temperature is only possible in exceptional cases because of the high irradiation damage of the specimen by 120 keV electrons. Most of the electron diffraction work was therefore performed at −130 °C. An example of such an electron diffraction diagram is displayed in Figure 4.

Table 2. Reflections of **3a** and **3b** in the Solid State at Room Temperature

$2\vartheta_{obsd}$ [deg]	$2\vartheta_{calcd}$ [deg]	d_{obsd} [Å]	indexing *hkl*	d_{calcd} [Å]	$2\vartheta_{obsd}$ [deg]	$2\vartheta_{calcd}$ [deg]	indexing *hkl*	d_{calcd} [Å]
		3a[a]					**3b**[b]	
1.56	1.609		100	54.9	1.52	1.414	100	62.5
		56.6			1.76	1.845	010	47.9
		48.2	010	46.9	2.12	2.162	$\bar{1}10$	40.9
2.34	2.258		$\bar{1}10$	39.1	2.48	2.476	110	35.7
		39.1			2.82	2.827	200	31.2
2.72	2.679		110	33.0	3.66	3.690	020	23.9
		33.2			3.82	3.762	$\bar{1}20$	23.5
3.30	3.219		200	27.4	4.24	4.242	300	20.8
		27.3			4.38	4.324	$\bar{2}20$	20.4
3.79	3.768		020	23.4	4.98	4.953	220	17.8
		23.3			5.44	5.494	030	16.1
4.22	4.343		120	20.3	5.78	5.690	400	15.5
		20.3			6.52	6.487	$\bar{3}30$	13.6
4.51	4.518		$\bar{2}20$	19.4				
		18.7						
4.80	4.829		300	18.2				
5.27	5.359		220	16.5				
		16.2						
5.53	5.653		030	15.6				
		15.4						
		13.7	400	13.7				
		12.7	$\bar{4}20$	12.8				
		11.7	040	11.7				
		10.3	240	10.2				
		9.3	600	9.1				
		8.1	440	8.2				

[a] Monoclinic lattice with the parameters $a = 55.7$ Å, $b = 47.6$ Å, $c = 4.8$ Å, $\gamma = 99.8°$, $Z = 2$ (c is inferred from electron diffraction). The data result in a density of $\rho = 1.17$ g cm^{-3}. (For this listing, two sets of data were used: diffractometer measurements are given by scattering angles of the reflections, and flatfilm Kiessig data are given by d values.) [b] Monoclinic lattice with the parameters $a = 62.7$ Å, $b = 48.7$ Å, $c = 4.8$ Å, $\gamma = 97.8°$, $Z = 2$ (c is inferred from electron diffraction). The data result in a crystalline density of $\rho = 1.16$ g cm^{-3}.
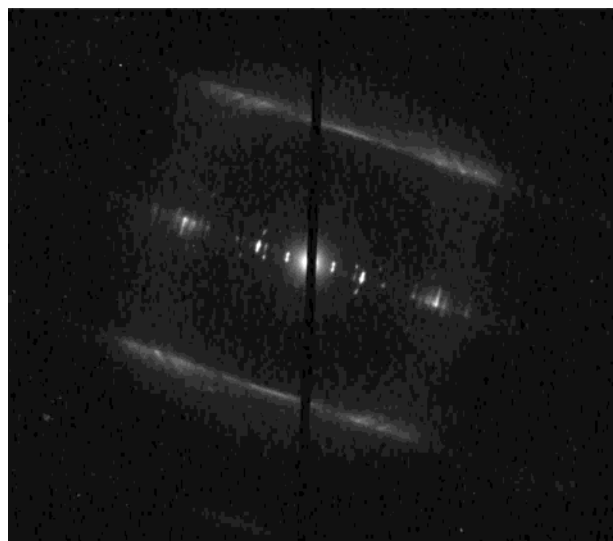
Figure 4. Electron diffraction pattern of a thin film of **3a**, recorded at −130 °C.

The electron diffraction pattern shows a fiberlike texture present in limited areas of a thin film. This observation supports not only the lattice symmetry for **3a** and **3b** as obtained from the X-ray data but also gives additional information on the packing behavior of the macrocycles within the crystal lattice. The continuous intensity along the layer lines, implying that adjacent stacks of macrocycles are not in register, is the

predominant feature of the electron diffraction pattern. In **3a**, more distinctly than in **3b**, some off-meridional sampling and even evident reflections on the layer lines are seen. This feature indicates that a herringbone structure is the most probable packing scheme in the solid. From this observation it can be inferred that the axis of the stacks is perpendicular to the plane of the basal oblique net, and this orientation is also suggested for the liquid crystalline state. The packing of the solid is then treated in terms of a monoclinic unit cell. In case of a herringbone structure, the normals to the planes of the macrocycles are oriented obliquely to the stack axis. The meridional distance corresponds for both **3a** and **3b** to a repeating period of 4.8 Å between two macrocycles along the stack axis. Some diffractograms of **3b** show a ring corresponding to a *d* value of 4.1 Å (Supporting Information). It originates certainly from the hexadecyl residues attached to the macrocycles, demonstrating that the aliphatic side chains are able to form crystallites as a function of crystallization kinetics. The side-chain crystallites are not oriented in-plane with the macrocycles; their function is more a space-filling one. This additional ring was never observed as a crystalline reflection for **3a**. In that case, sometimes a broad halo can be seen in the corresponding angular region. This observation is in agreement with the findings for a series of alkyl-substituted hairy rod polymers where separate alkyl crystallization is also a function of alkyl chain length for equal distances of attachment sites along the main chain.[25]

Solid-State NMR. Although a lattice symmetry with two symmetry-related units in a unit cell was discussed soon after the discovery of discotic liquid crystals, the restricted rotation of the molecules in the liquid crystalline state has only been rarely investigated.[20,26] The lower melting point of **3b** prompted us to perform advanced solid-state ^{1}H-^{13}C NMR investigations to gain further insight into the molecular dynamics of this macrocycle in the liquid crystalline phase. Fast magic-angle spinning (MAS) was applied,[27] together with standard dipolar decoupling[28] and recoupling[29] techniques, to ensure sufficient resolution of the ^{13}C resonance lines and to measure ^{1}H-^{13}C dipole−dipole couplings. On the basis of this spectral resolution, the segmental dynamics of individual CH$_n$ groups can be determined from ^{1}H-^{13}C dipole−dipole couplings that are subject to motional averaging effects. In 2D MAS NMR experiments, dipolar recoupling pulse sequences reintroduce ^{1}H-^{13}C dipole−dipole couplings for certain periods and generate characteristic spinning sideband patterns for all distinguishable CH$_n$ groups.[28] These sideband patterns are a sensitive measure for individual ^{1}H-^{13}C dipole−dipole couplings, which are then compared to coupling values of immobile segments, such as CH, CH$_2$, CH$_3$, or a phenyl ring, calculated from known ^{1}H-^{13}C bond lengths. Typically, an immobile C−H segment is characterized by a coupling of $D_{CH} = 21$ kHz, which is reduced when molecular motions occur on time scales below $\sim$10 μs, corresponding to a frequency range of >100 kHz.[30] By relating the measured

(reduced) dipolar coupling to the immobile case, a dynamic order parameter S can be determined for individual segments, where $S = 1$ represents a perfectly immobile segment and $S \rightarrow 0$ isotropic motion.

The dynamical properties of three different types of phenyl rings and several methyl groups in the macrocycle **3b** were investigated in the LC phase at 85 °C. The results are schematically summarized in Figure 5. Considering first the aromatic CH group (marked blue in Figure 5), a dipolar coupling of $D_{CH} = (21.0 \pm 0.5)$ kHz is extracted from the respective spinning sideband pattern (depicted in blue in Figure 5), which obviously agrees with the value of an immobile group. Hence, the phenyl ring is perfectly immobile on time scales below the millisecond range. In particular, there is no rotation of the macrocycles with frequencies above the kHz range in the columnar LC phase. Similar dynamics, i.e., overall molecular reorientations occurring at slower than kHz frequencies, were observed in the mesophases of phthalocyanines.[31]

Turning to the aromatic CH groups depicted in green in Figure 5, a reduced dipolar coupling of $D_{CH} = (16.4 \pm 0.5)$ kHz was measured, corresponding to a dynamic order parameter of $S \approx$ 0.80. This parameter indicates a small-angle motion of the phenyl ring with a mean excursion of $\pm15°$,[32] as indicated in Figure 5. A full rotation or a flip of the phenyl ring can be excluded, because it would lead to dipolar couplings significantly lower than the one observed. The dynamics of the OCH$_2$ group attached to the phenyl ring (marked red, together with the sideband pattern, in Figure 5) result in a residual coupling of $D_{CH} = (12.0 \pm 0.5)$ kHz, corresponding to $S \approx 0.55$. Assuming that the phenyl and OCH$_2$ motions are coupled but occur independently from each other, they can be separated by dividing the order parameters. Then, the OCH$_2$R segment exhibits an individual order parameter of $S \approx 0.70$. This segmental dynamics can be rationalized and illustrated in terms of a cone with an opening angle of $\pm20°$, which encompasses the core volume filled by the moving OCH$_2$R group.

Considering the oligo-alkyl substituents, a large mobility gradient was observed, starting with $S = 1$ at the immobile macrocyclic core and decreasing to $S < 0.1$ at the −CH$_2$CH$_3$ terminus of the alkyl chains (depicted in yellow in Figure 5). For the aromatic CH group within the substituent (marked purple in Figure 5) a residual dipolar coupling of $D_{CH} = (8.7$ kHz $\pm 0.5)$ kHz is determined. The corresponding dynamic order parameter, $S \approx 0.40$, can directly be related to a motion of the substituent as a whole, which occurs within a cone-shaped volume with an opening angle of $\pm30°$.

Thus, for different segments in the macrocycle **3b**, individual degrees of mobility could be determined by solid-state NMR, showing that the macrocyclic core is rather rigid in the liquid crystalline phase and does not rotate with kHz or higher frequencies within the column. The substituents, in contrast, show significant mobility above the kHz range, and their moving alkyl chains fill the space around the core. This combination of rigid and flexible parts within a macrocycle is essential for the formation of a thermotropic liquid crystalline phase. Moreover, the immobility of the rigid phenylethynyl core in the LC phase,

(25) (a) Stern, R.; Ballauff, M.; Lieser, G.; Wegner, G. *Polymer* **1991**, *32*, 2096−2105. (b) Cervinka, L.; Ballauff, M. *Colloid Polym. Sci.* **1992**, *270*, 859−872.
(26) Zamir, S.; Poupko, R.; Luv, Z.; Hüser, B.; Boeffel, C.; Zimmermann, H. *J. Am. Chem. Soc.* **1994**, *116*, 1973−1980.
(27) Schnell, I.; Spiess, H. W. *J. Magn. Reson.* **2001**, *151*, 153−227.
(28) Bennett, A. E.; Rienstra, C. M.; Auger, M.; Lakshmi, K. V.; Griffin, R. G. *J. Chem. Phys.* **1995**, 103, 6951.
(29) Saalwächter, K.; Schnell, I. *Solid State Nucl. Magn. Reson.* **2002**, *22*, 154−187.
(30) Brown, S. P.; Spiess, H. W. *Chem. Rev.* **2001**, *101*, 4125.

(31) Ford, W. T.; Sumner, L.; Zhu, W.; Chang, Y. H.; Um, P.-J.; Choi, K. H.; Heiney, P. A.; Maliszewskyj, N. C. *New J. Chem.* **1994**, *18*, 495−505.
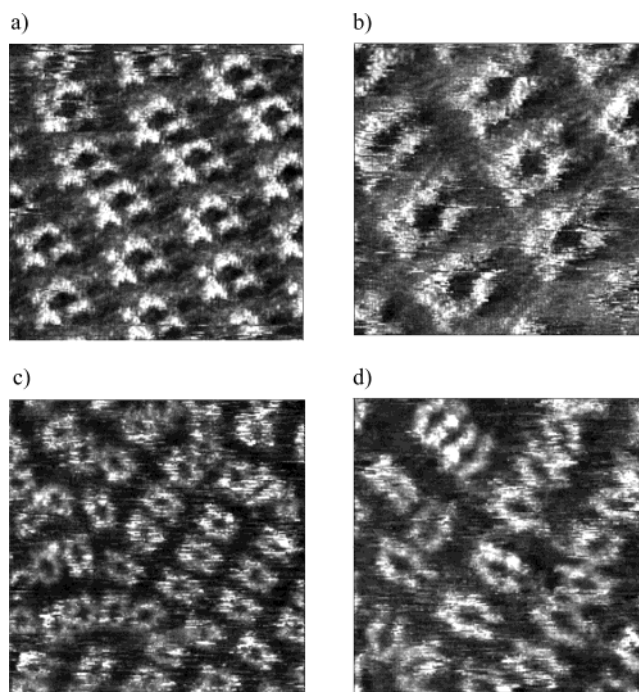(32) Hentschel, R.; Sillescu, H.; Spiess, H. W. *Polymer* **1981**, *22*, 1516−1521.
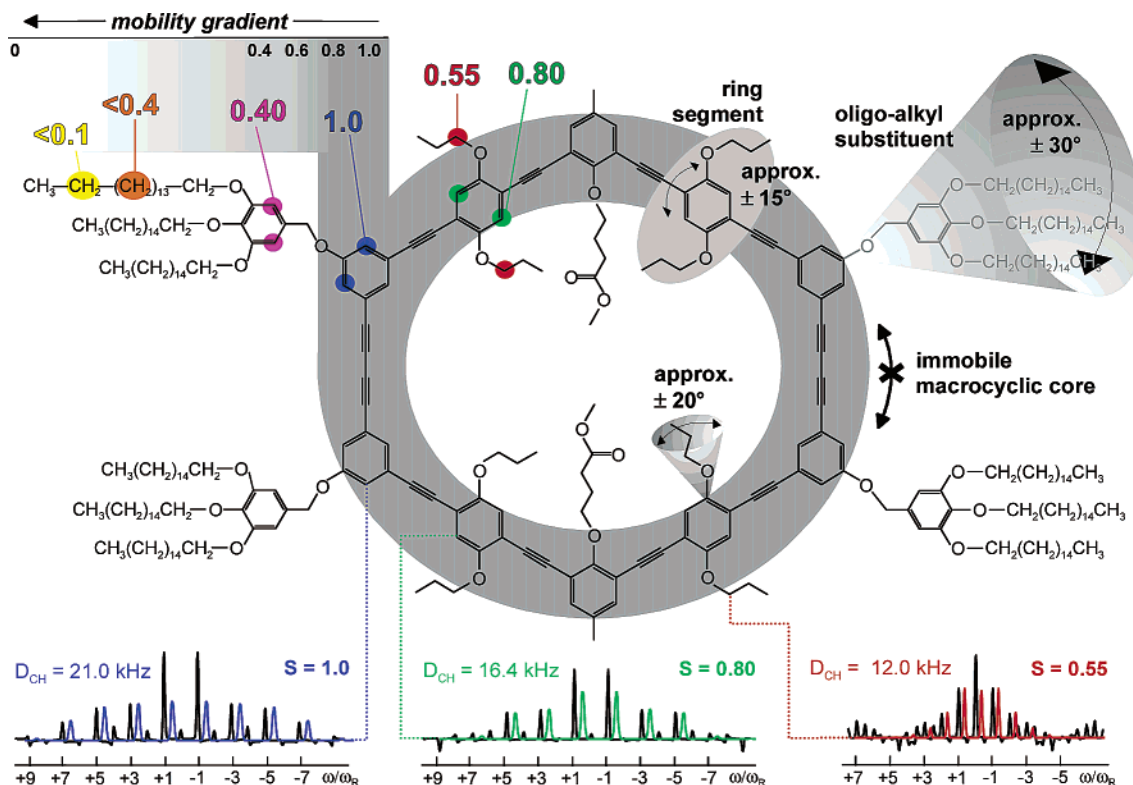
Figure 5. Schematic representation of the segmental dynamics (faster than kHz frequencies) in **3b**. On the left, the degree of mobility for individual segments is given by the respective dynamic order parameter, *S*, while on the right the corresponding motions are depicted. At the bottom, three examples of spinning sideband patterns are given, from which the residual ^{1}H-^{13}C dipolar couplings and the corresponding segmental dynamics are extracted (left and middle: HDOR patterns, right: REREDOR pattern; the experiments are described in detail in ref 29). The black and colored lines represent experimental and fitted data, respectively.

as determined from the NMR experiments, is consistent with the observation that the unit cell of the basal net contains two symmetry-related units, as determined by the X-ray experiments.

Adsorption. As indicated before, there is a considerable interest in the investigation of the 2D ordering of the macrocycles because nanopatterns and functionalized nanopatterns may provide a tool for the formation of supramolecular 3D structures by epitaxial growth.[33] One common technique for the investigation of 2D ordering of these macrocycles at the liquid– solid interface is scanning tunneling microscopy (STM).[34] For this purpose, the macrocycles were dissolved in phenyloctane, and a drop of the solution was brought onto a freshly cleaved HOPG surface. The STM investigations were then performed at the liquid–solid interface.[11j,13,35]

Figure 6 is a set of STM pictures of **3a** and **3b** at the liquid (1-phenyloctane)–solid (graphite) interface. The brightness refers to the level of the detected tunneling current. Aromatic and conjugated parts of molecules are known to show a higher tunneling efficiency than the aliphatic alkyl parts.[36] Therefore, the bright parts can be attributed to the shape-persistent

(33) (a) Zeng, C.; Wang, B.; Li, B.; Wang, H.; Hou, J. G. *Appl. Phys. Lett.* **2001**, *79*, 1685–1688. (b) Abdel-Mottaleb, M. M. S.; Schuurmans, N.; De Feyter, S.; van Esch, J.; Feringa, B. L.; De Schryver, F. C. *Chem. Commun.* **2002**, 1894–1895. (c) Hoeppener, S.; Wonnemann, J.; Chi, L.; Erker, G.; Fuchs, H. *ChemPhysChem* **2003**, *4*, 490–494. (d) Hoeppener, S.; Chi, L.; Fuchs, H. *ChemPhysChem* **2003**, *4*, 494–498.
(34) Rabe J.; Buchholz, S. *Science* **1991**, *253*, 424–427.
(35) Krömer, J.; Rios Carreras, I.; Fuhrmann, G.; Musch, C.; Wunderlin, M.; Debaerdemaeker, T.; Mena-Osteritz, E.; Bäuerle, P. *Angew. Chem.* **2000**, *112*, 3623–3628; *Angew. Chem., Int. Ed.* **2000**, *39*, 3481–3486.
(36) De Feyter, S.; Gesquière, A.; Abdel-Mottaleb, M. M. S.; Grim, P. C. M.; Meiners, C.; Sieffert, M.; Valiyaveettil, S.; Müllen, K.; De Schryver, F. C. *Acc. Chem. Res.* **2000**, *33*, 520–531.

Figure 6. STM images of **3a** (a, b) and **3b** (c, d) at the liquid (1-phenyloctane)–solid (graphite) interface. (a) 17.7×17.7 nm^2, $I = 0.65$ nA; $V = -0.714$ V. (b) 12.7×12.7 nm^2, $I = 0.8$ nA; $V = -0.784$ V. (c) 25.9×25.9 nm^2, $I = 0.35$ nA; $V = -0.926$ V. (d) 18×18 nm^2, $I = 0.35$ nA; $V = -1.208$ V.

backbone of the compounds. The molecular dimensions observed here correspond well with those obtained by single-crystal X-ray analysis of similar macrocycles. In addition, the

contrast within a macrocycle correlates with the density of the highest occupied molecular orbital (HOMO) of the macrocycle, as we have described before.[13] Moreover, the presence of the four exo phenyl rings carrying the alkyl chains stresses the long axis of the molecules and allows the determination of the orientation of the macrocycles on the graphite support in a straightforward fashion. The dark areas between the macrocycles are occupied by alkyl chains. In a few cases, their orientation could be determined. As is often the case, they are oriented along one of the main symmetry axes of graphite. The interior of the macrocycles remains dark, and no details of the intraannular groups can be observed.

In contrast to the data published on **1c**,[13] **3a** and **3b** do not tend to form extended well-defined 2D arrays. Although local ordering is found to a certain degree, the rings do not form a 2D crystal. However, the extent of ordering depends on the solvent used for the investigations. When physisorbed from a 1,2,4-trichlorobenzene solution, the degree of ordering is often more pronounced (although far from ideal) compared to images obtained for monolayers physisorbed from 1-phenyloctane, although the image resolution is worse (see Supporting Information). Several factors can contribute to this lack of long-range ordering. Imaging occurs at rather high set point values (see figure captions), which leads to an increased interaction with the macrocycles. However, repeated scanning does not affect the relative orientation of the macrocycles. In our opinion, the main reason for the lack of long-range order is the balance or competition between kinetically and thermodynamically controlled monolayer formation. The interplay between the solute—solvent interaction and the solute—substrate interaction will play an important factor. Both molecules contain 12 long alkyl chains, which will lead to a considerable interaction with the graphite substrate upon adsorption (in addition to the interaction between the aromatic cores and the substrate). Even if the molecule is not packed in an ideal fashion, the molecules—substrate interaction will be large enough to immobilize the molecules to a certain degree on the substrate, and as such, they can be kinetically trapped. Given that 1,2,4-trichlorobenzene is a better solvent for the macrocycles than 1-phenyloctane, the extent of kinetic trapping will be less in 1,2,4-trichlorobenzene, leading, on the time scale of the experiment, to more long-range ordered systems. Further investigations will therefore also deal with optimization of the physisorption protocol, which includes, among other parameters, a variation of the solvent, temperature, and concentration. Nevertheless, for **3a** the lattice constants of a 2D unit cell of oblique symmetry were extrapolated to be in the order of $A = 3.4$ nm, $B = 5.2$ nm, and $\Gamma = 87°$. Although these parameters cannot be obtained with accuracy, they show a similar molecular size of **1c** and **3a** on the graphite. In comparison to the basal net a and b of the 3D structure of **3a**, the distinctive feature between the two piles of macrocycles is lost by the induced parallelism of rings and substrate. Therefore, the lattice parameter recognizable on the STM pattern of the surface is considerable smaller.

Macrocyclic esters **3a** and **3b** are examples of the extension of the concept of nanopatterning toward nanofunctionalization of the HOPG surface in the multinanometer regime. The use of these surfaces for the formation of supramolecular 3D structures is in progress.

Summary

In summary, we have presented the synthesis of the shape-persistent macrocycles **3a** and **3b** with extraannular oligo-alkyl substituents and intraannular polar groups which can be viewed as intraannular filled analogues of the previously reported macrocycles **1**. The macrocycles **1** do not exhibit a stable liquid crystalline phase and several arguments indicate that the large internal void of the macrocycles **1** is responsible for that. However, the incorrect balance between the dimensions of the core and the flexible periphery might have been an alternative explanation. The investigation of the thermal behavior of **3a** and **3b** has shown that both compounds exhibit stable columnar mesophases (as revealed by optical microscopy, X-ray and electron diffraction studies, and solid-state NMR), showing that the balance between the rigid and the flexible parts in **1** and **3** was correct. This finding is another support for our hypothesis that the large internal void in nanometer-size shape-persistent macrocycles destabilizes a thermotropic mesophase. Apart from their thermotropic behavior, the adsorption of **3a** and **3b** on HOPG has been investigated. The compounds form monolayers on the graphite, and their 2D ordering was investigated by STM, indicating that the macrocycles allow not only the formation of nanostructured surfaces but also the creation of functionalized nanostructured surfaces.

Experimental Section

Synthesis. Compounds **6** and **9** were prepared according to literature procedures.[13] For synthetic procedures and analytical data for all other compounds, please see the Supporting Information.

X-ray Scattering and Electron Diffraction. Temperature-dependent X-ray scattering was mainly performed on a homemade 2-circle diffractometer (Huber) in transmission mode. The diffractometer was equipped with a germanium monochromator enabling the separation of the copper K_α dublett, using for the measurement $CuK_{\alpha1}$ with $\lambda = 1.5406$ Å. For data recording, a position-sensitive 120° Inel detector was used. Electron diffraction of the solid compound was performed in a LEO 912 transmission electron microscope with an integrated electron energy loss spectrometer at a high voltage of 120 kV. Thin films were prepared from solution and transferred to carbon-coated supporting grids prior to being molten and subsequently recrystallized on the carbon film (electron diffraction on films in the liquid crystalline state was not possible because of the very high irradiation damage at elevated temperatures).

Solid-State NMR. Data were collected on a Bruker DRX spectrometer with a 16.4 T magnet (700 and 176 MHz for ^{1}H and ^{13}C, respectively). A double resonance MAS (magic-angle spinning) probe was used, allowing MAS frequencies of 30 kHz. The samples ($\sim$15 mg) were packed into rotors of 2.5-mm outer diameter. The spectra are referenced to adamantane (1.63 ppm for ^{1}H, and 38.5 ppm for ^{13}CH).

STM Investigation. Experiments were performed using a Discoverer scanning tunneling microscope (Topometrix Inc. Santa Barbara, CA) with a typical frame acquisition time of 7 s, along with an external pulse/function generator (model HP 8111 A), with negative sample bias. Tips were etched electrochemically from Pt/Ir wire (80%/20%, diameter 0.2 mm) in a 2 N KOH/6 N NaCN solution in water. Prior to imaging, the compound under investigation was dissolved in 1-phenyloctane or 1,2,4-trichlorobenzene (Aldrich), and a drop of this solution (0.1 wt %) was applied on a freshly cleaved surface of HOPG. The STM investigations were then performed at the liquid—solid interface. The presented STM images were acquired in the variable current mode (constant height) under ambient conditions. In the STM images, white corresponds to the highest and black to the lowest measured tunneling current. The experiments were repeated in several sessions using

different tips to check the reproducibility and to avoid artifacts. After registration of an STM image of the monolayer structure, the underlying graphite lattice was recorded at the same position by decreasing the bias voltage, serving as an in situ calibration. All STM images contain raw data and are not subjected to any manipulation or image processing.

Supporting Information Available: Synthetic procedures and analytical data for the compounds prepared (PDF). This material is available free of charge via the Internet at http://pubs.acs.org.

JA038484X